



# Topological semimetal driven by strong correlations and crystalline symmetry

Lei Chen<sup>1</sup>, Chandan Setty<sup>1</sup>, Haoyu Hu<sup>1</sup>, Maia G. Vergniory<sup>2,3</sup>, Sarah E. Grefe<sup>4</sup>, Lukas Fischer<sup>5</sup>, Xinlin Yan<sup>5</sup>, Gaku Eguchi<sup>5</sup>, Andrey Prokofiey<sup>5</sup>, Silke Paschen<sup>1,5</sup>, Jennifer Cano<sup>6,7</sup> and Oimiao Si<sup>1</sup>

Electron correlations amplify quantum fluctuations and, as such, are recognized as the origin of many quantum phases. However, whether strong correlations can lead to gapless topological states is an outstanding question, in part because many of the ideas in topological condensed-matter physics rely on the analysis of an effectively non-interacting band structure. Therefore, a framework that allows the identification of strongly correlated topological materials is needed. Here we suggest a general approach in which strong correlations cooperate with crystalline symmetry to drive gapless topological states. We test this materials design principle by exploring Kondo lattice models and materials whose space-group symmetries promote different kinds of electronic degeneracies. This approach allows us to identify Weyl-Kondo nodal-line semimetals with nodes pinned to the Fermi energy, demonstrating that it can be applied to discover strongly correlated topological semimetals. We identify three heavy-fermion compounds as material candidates, provide direct experimental evidence for our prediction in Ce, Au, In. and discuss how our approach may lead to many more. Our findings illustrate the potential of this materials design principle to guide the search for new topological metals in a broad range of strongly correlated systems.

lectron correlations and topology are well established as engines for surprising and potentially functional properties. Strong correlations promote quantum fluctuations, which engender abundant phases of matter and various quantum phase transitions<sup>1,2</sup>. Meanwhile, extensive developments have taken place in non-interacting electron systems, especially those with sizable spin-orbit couplings (SOCs). In particular, the role of space-group (SG) symmetry in determining and classifying symmetry-protected topological phases has been highlighted<sup>3-7</sup>. In the archetypal version of two-dimensional (2D) and three-dimensional (3D) topological semimetals, SG symmetry enforces Dirac nodes in the honeycomb lattice (as realized in graphene<sup>8</sup>) and diamond lattice<sup>9</sup>, respectively. These understandings set the stage for a systematic search of weakly correlated topological materials in terms of the constraints of SG symmetries on non-interacting band structures for a variety of crystal structures, which has led to a large topological materials

We can expect that the intersection of these two fields will be especially fertile in breeding novel quantum phases, but it remains a largely open terrain<sup>12–14</sup> especially for the case with gapless bulk excitations<sup>2,15</sup>. The fractional quantum Hall effect amply demonstrates the capability of strong correlations to drive gapped topological states. By contrast, correlated gapless electronic topology has been much less explored. The usual approach starts from non-interacting symmetry-protected topological states. It considers the interactions as a perturbation or as producing a symmetry-breaking ordered state—such as a magnetic order—that, in turn, modifies the weakly correlated topology<sup>16</sup>. In the opposite limit, where the electrons' correlations dominate over their kinetic energy, there has been a  $considerable \ lack \ of \ strongly \ correlated \ gapless \ topological \ materials.$ It is pressing to realize such materials, which are important in their

own right and may also serve as anchoring points to explore the overall landscape of strongly correlated gapless topology. Recently, a non-perturbative study has led to a Weyl-Kondo semimetal phase<sup>17-19</sup> in a toy model associated with the diamond lattice. Concurrently, such a phase was experimentally advanced in a cubic heavy-fermion compound Ce<sub>3</sub>Bi<sub>4</sub>Pd<sub>3</sub> based on the measurements of specific heat and spontaneous Hall effect<sup>20-22</sup>. The interplay between substantial electron correlations and lattice geometry is also being experimentally explored in other materials such as kagome metals<sup>23-25</sup>.

These developments motivate the search for a general nonperturbative framework to treat the interplay of correlation and topology and design both phases and materials of correlated gapless electronic topology. Our hypothesis is that strong correlations cooperate with crystalline symmetry to produce such states. Specifically, as Fig. 1a illustrates, strong correlations give rise to emergent excitations at low energies. The SG symmetry constrains these excitations, leading to emergent topological phases and enforcing their gapless nature. If validated, the proposition provides a materials design principle for correlated gapless electronic topology. Still, the proposed cooperation is counterintuitive, because strong correlations tend to cause localization and gap out electronic excitations<sup>26,27</sup>.

To test the proposed materials design principle, it is important to go beyond toy models and explore correlated systems with general SG symmetries that may promote different types of nodal electronic state. We illustrate our approach by narrowing down the choice of strong-coupling models for our study here as follows. We focus on SG symmetries where electronic degeneracies may develop at partial fillings, regardless of orbital content. These often happen in non-symmorphic SGs. We examine the case where interactions do not break crystalline or time-reversal symmetries, as a point of principle. Finally, to be definite, we formulate our materials design

Department of Physics and Astronomy, Rice Center for Quantum Materials, Rice University, Houston, TX, USA. 2Max Planck Institute for Chemical Physics of Solids, Dresden, Germany. 3Donostia International Physics Center, Donostia-San Sebastian, Spain. 4Theoretical Division, Los Alamos National Laboratory, Los Alamos, NM, USA. 5 Institute of Solid State Physics, Vienna University of Technology, Vienna, Austria. 6 Department of Physics and Astronomy, Stony Brook University, Stony Brook, NY, USA. 7Center for Computational Quantum Physics, Flatiron Institute, New York, NY, USA. e-mail: paschen@ifp.tuwien.ac.at; jennifer.cano@stonybrook.edu; gmsi@rice.edu

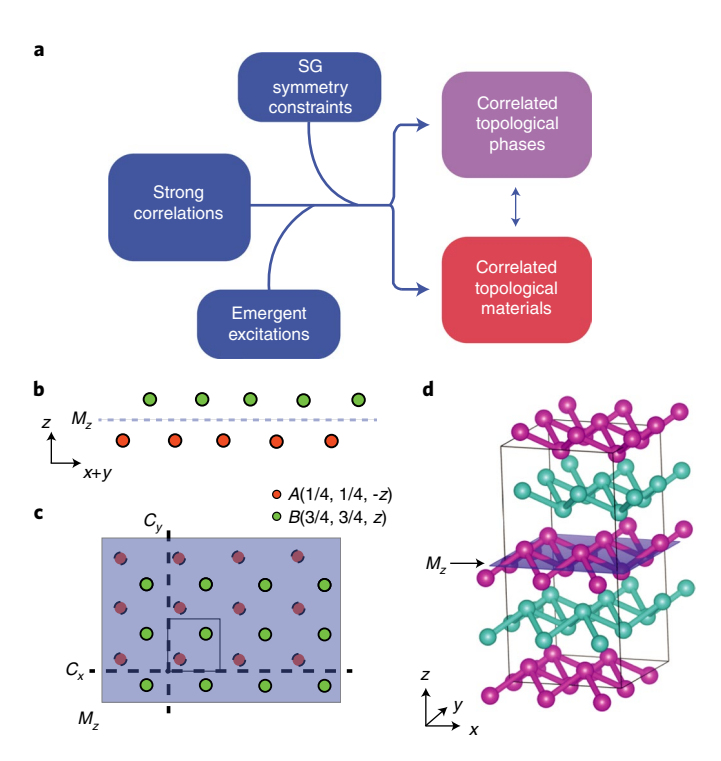


**Fig. 1** | Materials design principle and SG symmetry. **a**, Proposed cooperation between strong correlations and SG symmetry in realizing correlated gapless topological states and materials. Here low-energy excitations emerge from strong correlations and are subjected to SG symmetry constraints, leading to correlated topological phases in theoretical models and materials that realize such phases. **b,c**, Lattice structure of the square-net layer with sublattices A and B on Wyckoff position B0. Also shown are the mirror B1 and screw B2 and B3 non-symmorphic symmetries. **d**, B3 structure.

in the context of Kondo lattice systems, as realized via the limit of strong Coulomb repulsion in periodic Anderson models. The Kondo effect leads to a ground state in which the local moments and conduction electrons entangle and form a spin singlet, which supports composite fermions in the excitation spectrum at low energies—within the Kondo energy scale of Fermi energy<sup>28–30</sup>. Generalizations to other correlated systems will be discussed.

We, thus, consider a Kondo lattice system that contains mirror symmetry, which is known to favour Weyl nodal lines in noninteracting systems<sup>31–34</sup>. Our focus is on the non-symmorphic and non-centrosymmetric square-net systems, which host both mirror and screw non-symmorphic symmetries (Fig. 1b,c). Especially, SG 129 has been a fertile setting for the electronic degeneracies of non-interacting systems<sup>35-40</sup> and is particularly advantageous in that the degeneracies are orbital independent<sup>4</sup>. Allowing for inversion-symmetry breaking, we demonstrate the cooperation of strong correlations with SG symmetry in producing a novel phase a Weyl-Kondo nodal-line semimetal. Our analysis of correlationdriven topological semimetal phases gives rise to a general procedure to design new materials that realize such phases. We illustrate this materials design principle by identifying several new candidate Ce-based correlated topological semimetals, and indicate how it can be used to identify many new materials.

The periodic Anderson model is specified by the following Hamiltonian:

$$\mathcal{H} = \mathcal{H}_d + \mathcal{H}_{cd} + \mathcal{H}_c. \tag{1}$$

The spin-1/2 d- and c-fermion operators describe the physical localized f electrons and the light spd conduction electrons that form the non-interacting bands, respectively. Further details of the model and solution method are described in the Methods.

The 3D crystalline structure of SG 129 (P4/nmm) and its inversion-breaking counterpart, SG 31, are constructed by stacking 2D layers in the z direction. To set the stage for analysing the interplay between SG symmetry and correlation effects, we start from this 2D system corresponding to the layer group p4/nmm. The Hamiltonian of the contesponding to the kye group P Hamiltonian of the contesponding to the  $\mathcal{H}_c$  is described in a matrix form:  $\mathcal{H}_c = \sum_{\mathbf{k}} \Psi_{\mathbf{k}}^{\dagger} H_c(\mathbf{k}) \Psi_{\mathbf{k}}$ , where  $\Psi_{\mathbf{k}}^{\mathrm{T}} = (c_{\mathbf{k} \uparrow A}, c_{\mathbf{k} \downarrow A}, c_{\mathbf{k} \uparrow B}, c_{\mathbf{k} \downarrow B})$ , A and B are two sublattices,  $\mathbf{k}$  is the wavevector and  $\sigma = \uparrow$  or  $\downarrow$ denotes the spin quantum numbers. As described in the Methods (and Supplementary Fig. 3), it contains tight-binding hopping terms between the nearest  $(t_1)$  and next-nearest  $(t_2)$  neighbours, an SOC ( $t^{SO}$ ) term and an inversion-symmetry-breaking ( $\Delta$ ) term. In the absence of the Kondo effect, all the electrons prefer to occupy the low-lying d states to half-filling, making the d component to be a Mott insulator. Concomitantly, the conduction c-electron bands are completely empty, that is, they lie above the Fermi energy. Figure 2a shows the band structure for the case of the inversion-symmetry-breaking potential  $\Delta = 0$ , that is, in the presence of the full p4/nmm symmetry. The mirror and screw non-symmorphic symmetries enforce additional crossings at high-symmetry points X, Y and M (Methods)<sup>35</sup>. Since these Dirac points occur far above the Fermi energy, they leave the ground state topologically trivial. We note that the separated d-electrons are deep levels far away (below) the Fermi energy; they are half-filled and form a Mott insulator due to the large onsite Coulomb repulsion. Supplementary Fig. 1a shows the dispersion of the Kondo-driven Fermi-energy-bound composite fermions for  $\Delta = 0$ . Because the composite-fermion bands are subjected to the non-symmorphic symmetry constraint, they feature Dirac nodes at X, Y and M.

We are now in position to present our main results on the 3D SGs 129 and 31. For SG 129, the mirror and screw symmetries have the same effect as in the 2D case. This implies that Kondo-driven dispersive Dirac nodes robustly develop along the XR, MA and YS lines in the composite-fermion spectrum within the Kondo energy of the Fermi energy. Their dispersive nature implies that a Dirac nodal point can develop at the Fermi energy. We illustrate this point through a concrete calculation (Supplementary Fig. 2a,b). We note that in the presence of a magnetic field (or ferromagnetic order), Kondo-driven Weyl nodes develop (Supplementary Fig. 2c,d).

The case of SG 31 is more involved. To be definite, we consider the  $\mathcal{AA}$  stacking of square-net layers (Fig. 1d) with the two stacking layers hosting s and p orbitals, respectively<sup>32,33</sup>. The corresponding periodic Anderson model is given in the Methods. In the presence of the Kondo effect, our results are shown in Fig. 3a. Nodes develop in the dispersion of the Kondo-driven composite fermions, which are more clearly seen in the zoomed-in view of the immediate vicinity of the Fermi energy (Fig. 3b). In our model, the Kondo-driven nodes are precisely at  $E_{\rm P}$ . These electronic degeneracies appear in the form of Weyl nodal lines in the  $k_z$ =0 plane (Fig. 3c). All these reflect the mirror non-symmorphic  $\{M_z|\frac{1}{2},\frac{1}{2}0\}$  symmetry. Because they are associated with the highly renormalized composite fermions, the Weyl nodal-line excitations have strongly reduced velocities. We stress that the nodal lines are robust against the SOC.

The realization of the Weyl–Kondo nodal-line semimetal is particularly important, as it suggests the emergence of drumhead surface states. We have computed the excitation spectrum on the (001) face in a slab with 40 unit cells. As indicated in Fig. 3d, we find Kondo-driven drumhead surface states that are bounded by the projections of the Weyl rings. Importantly, the dispersion of the drumhead states also captures the Kondo energy scale and hence is strongly correlation renormalized.

NATURE PHYSICS ARTICLES

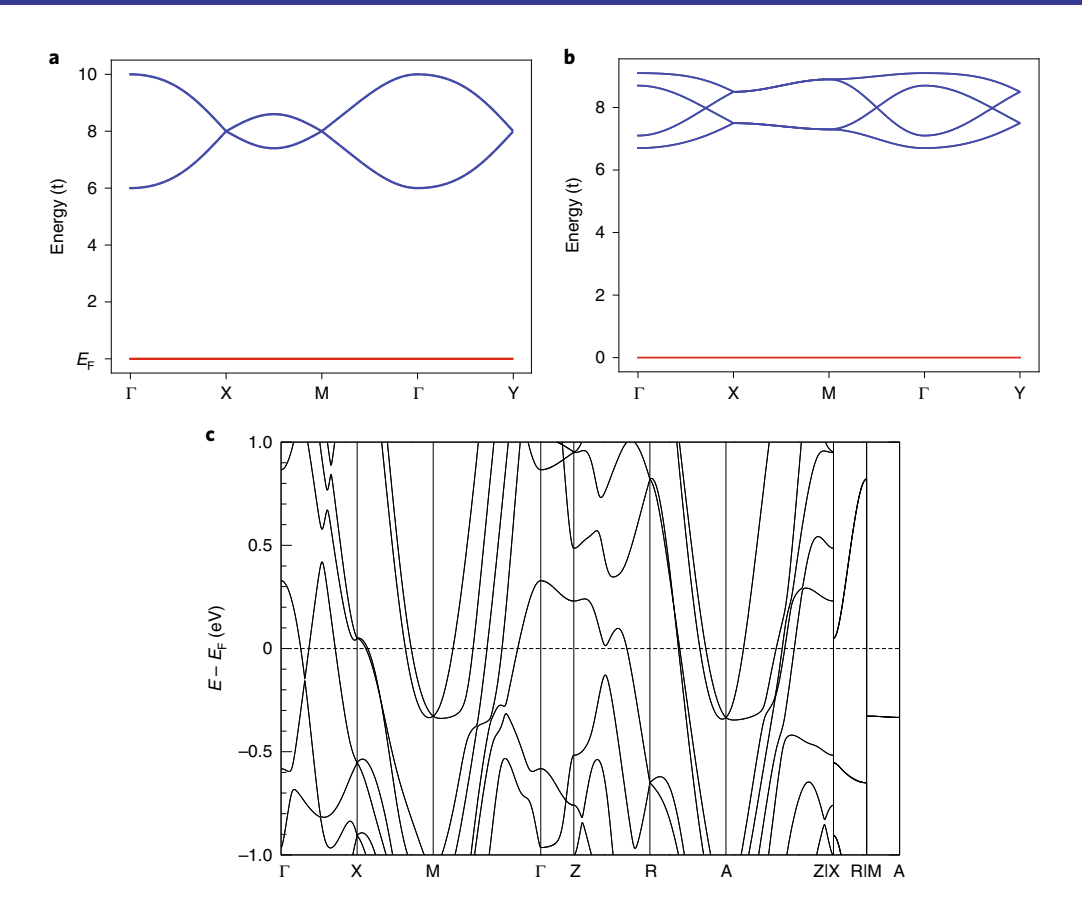


**Fig. 2** | **Electronic structure in the absence of Kondo effect. a**, Dispersion of a 2D square net with  $(t_1, t_2, t^{SO}) = (1.0, 0, 0.6)$ . The line at  $E_F$  illustrates the localized electrons. The fourfold degeneracies of the conduction bands occur at high-symmetry points X, Y and M away from the Fermi energy. **b**, Dispersion of the 3D-stacked square net without either inversion-symmetry breaking or SOC. The parameters are  $(t_1, t_2, t_2^1, t_2^2, \Delta_Z) = (1.0, 0.4, 0.3, 0.3, 0.8)$ . **c**, Band structure of the conduction spd electrons of  $CePt_2Si_2$ , as determined by f-core DFT calculations. Symmetry-dictated Dirac nodes appear at X and M (and R and A) away from the Fermi energy, as captured by the model dispersions in **a** and **b**.

We now turn to the experimental signatures of the Kondo-driven Weyl nodal-line semimetals. The first category of signatures bears similarities with those of the Weyl–Kondo semimetals<sup>17–22</sup>. For example, because the velocity  $v^*$  is highly reduced from the typical bare conduction-electron value v, the specific heat is expected to have a quadratic temperature dependence with a large enhancement factor (Supplementary Information):

$$c_{\nu} = \Gamma T^2. \tag{2}$$

Here the prefactor is  $\Gamma = \frac{K}{2\pi} \frac{9\zeta(3)}{2} \left(\frac{k_{\rm B}}{\hbar \nu^*}\right)^2 k_{\rm B}$ , where K is the length of the nodal line,  $\hbar$  is the Planck's constant divided by  $2\pi$ ,  $k_{\rm B}$  is the Boltzmann constant, and zeta function  $\zeta(3) \approx 1.202$ . It is enhanced from the typical non-interacting value by  $(\nu/\nu^*)^2$ , which is of the order of  $(W/k_{\rm B}T_{\rm K})^2$ , where W is the bare conduction-electron bandwidth. This enhancement factor is huge—about  $10^4-10^6$  for moderately to strongly renormalized heavy-fermion semimetals. As another example, the enhanced Berry curvature near the Fermi energy can be probed through the spontaneous Hall effect<sup>21</sup>.

The second category of experimental signatures is distinct for the Kondo-driven nodal-line phase. As one example, the nodal lines lead to a non-trivial Berry phase of any closed loop perpendicular to the mirror plane. The resulting characteristic signatures in quantum oscillations for such a strongly correlated setting are considerably more challenging to probe than their weakly correlated counterparts<sup>41–43</sup>. However, in materials with moderate mass enhancement (as we will identify below), these experiments are expected to be

feasible. As another example, the drumhead surface states will lead to distinct spectroscopic signatures. As in weakly correlated systems<sup>44</sup>, they can, in principle, be probed by quasiparticle interference measurements via scanning tunnelling microscopy; here the quasiparticle interference pattern develops a structure at wavevectors whose magnitude is bounded from above by the location of the nodal lines in the bulk, as well as at energies that are bounded above by the bandwidth of the drumhead states<sup>45</sup>. Finally, the developments of recent years<sup>46</sup> make angle-resolved photoemission spectroscopy as a promising probe of the dispersive bulk and surface *f*-electron states that we have discussed.

Next, we turn to demonstrate how our approach guides the search for new correlation-driven topological materials. Because the composite fermions must be located near the Fermi energy, we can expect the Kondo-driven semimetal phases to host topological nodal excitations near the Fermi energy for generic fillings. Consequently, the cooperation of symmetry and Kondo correlation is adequate to realize candidate Kondo materials; this general procedure is outlined in Fig. 1a. In passing, we note one general point. Designing strongly correlated topological materials is inherently difficult; in the presence of strong correlations, the ab initio calculations of electronic states represent a challenge. Here we bypass this difficulty by using symmetry. Our results on the Kondo-lattice model Hamiltonians imply that SG symmetry and Kondo correlation cooperate in driving correlated topological semimetals. Hence, we can design new materials for correlation-driven topological semimetals purely based on crystalline symmetry and strong

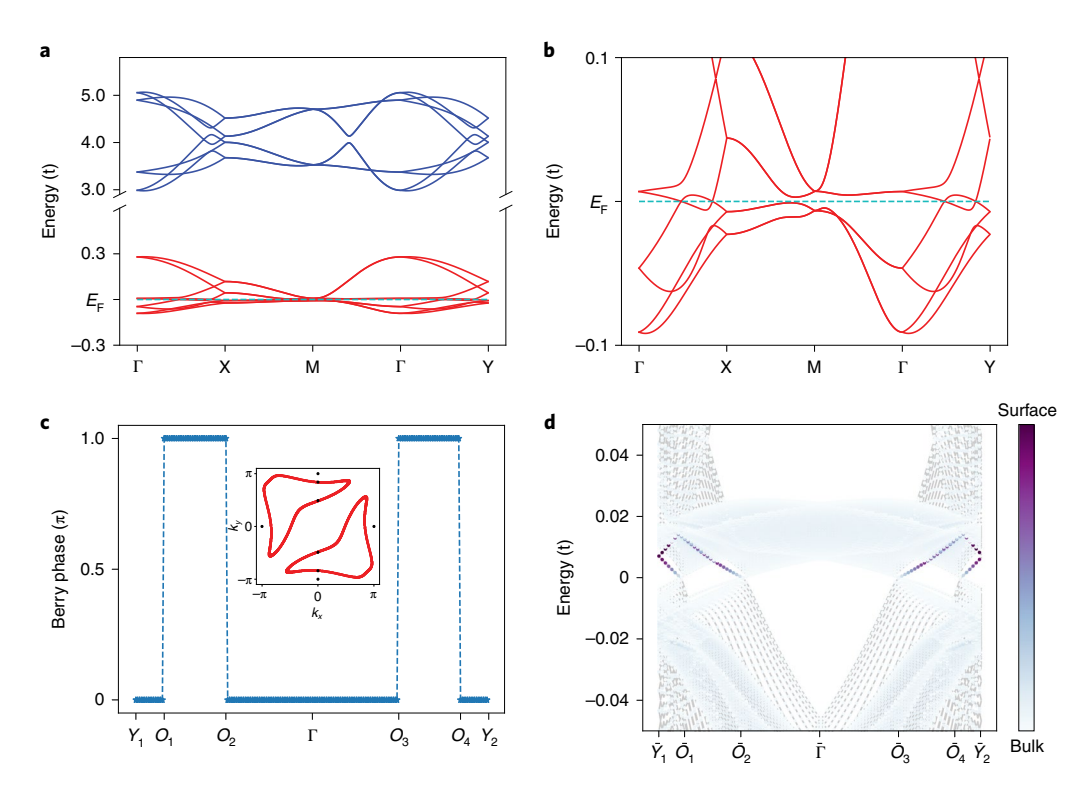


**Fig. 3 | Kondo-driven composite fermions of 3D-stacked square nets with broken inversion symmetry. a**, Dispersion, including the composite fermions (the lower red part), within the  $k_z$  = 0 plane. Here V = 3, in the unit of  $t_1$  that is set to 1. The other parameters are set to  $(t_2, \Delta, t_2^1, t_2^2, \Delta_z, m_z, E_d, \mu)$  = (0.4, 0.4, 0.3, 0.3, 0.8, 0.08, -2, -3.730). The parameters were chosen without any fine-tuning; the only requirement is that  $r_1$  and  $r_2$  are found to be non-zero. The saddle-point analysis yields  $(r_1, r_2, l_1, l_2)$  = (0.498, 0.374, -2.820, -2.294). **b**, Zoomed-in dispersion of the Kondo-driven composite fermions. **c**, Berry phase (in the z direction) of the Kondo-driven Weyl nodal lines for fixed  $k_x$  = 0;  $O_{1,2,3,4}$  mark the points of intersection with the nodal lines (Supplementary Fig. 3c). The inset shows the Kondo-driven Weyl nodal lines in the  $k_z$  = 0 plane. **d**, Kondo-driven drumhead surface states. The momentum-resolved surface density of states are shown for the spectrum close to the Fermi energy on the (001) surface along  $Y_1(0, -\pi)$  to  $Y_2(0, \pi)$ . A bar atop the momentum represents its projection onto the surface.

correlations, without resorting to ab initio results for the correlated electronic structure

We first consider SG 129, and focus on the case of Ce ions on site 2c. The procedure is outlined in Fig. 4a and further described in Supplementary Fig. 4. It leads to two new materials, namely, CePt,Si, and CeRh<sub>2</sub>Ga<sub>2</sub>, which we propose to realize the Kondo-driven semimetal phase. Both remain paramagnetic down to the lowest temperature of somewhat below 2 K (refs. 47,48) that has been experimentally measured, and both have strong correlations as inferred from their moderately enhanced specific heat (Supplementary Information). Moreover, both show semimetallic behaviour. Below their respective Kondo temperatures, their resistivity as a function of temperature (Supplementary Fig. 5a,b) behaves similarly as the well-established heavy-fermion semimetals Ce<sub>3</sub>Bi<sub>4</sub>Pd<sub>3</sub> and CeNiSn (refs. 20,49), respectively (Supplementary Fig. 5c,d). For CePt<sub>2</sub>Si<sub>2</sub>, the spd electronic structure, determined by f-core density functional theory (DFT) calculations (Methods), are displayed in Fig. 2c. Evidently, the symmetry of SG 129 dictates the existence of Dirac nodes at the X, M, R and A points, which are located away from the Fermi energy. The results for CeRh<sub>2</sub>Ga<sub>2</sub> are similar (Supplementary Fig. 7). The DFT-calculated electronic structure is expected to apply well above the Kondo temperature. Below their respective Kondo temperatures, the approach we have advanced here suggests that they will realize Kondo-driven topological semimetals. The precise nature of the renormalized band structure requires the construction of tight-binding representations of the DFT-derived band structure and the ab initio input of Kondo couplings. We outline how this construction can be done in the Supplementary Information and Supplementary Fig. 8, and reserve the correlated ab initio studies

for a future work. Still, our solution of the Kondo-lattice model Hamiltonian with SG 129 and the resulting conclusion about the cooperation between symmetry and Kondo correlation imply that both materials qualify as candidates for the correlation-driven topological semimetals advanced here.

Studies of these materials set the stage to search for additional strongly correlated semimetals. In the case of a non-zero inversion-symmetry-breaking term  $\Delta$ , corresponding to SG 31, a similar search procedure for the Ce-based case is outlined in Fig. 4b and Supplementary Fig. 4. It leads to the identification of a new material,  $Ce_2Au_3In_5$ , as a candidate heavy-fermion material that is known not to order down to the lowest measured temperature  $(2\,K)^{50}$ . Its inversion-symmetry breaking is illustrated in Fig. 4e. We propose it as a candidate material to realize the Weyl–Kondo nodal-line semimetal advanced here. Thus, the considerations of these two specific SGs lead to the identification of three new candidate Kondo-driven topological semimetals (Fig. 4c). This result already considerably expands the material base for such strongly correlated topological semimetals beyond the known case of  $Ce_3Bi_4Pd_3$  (refs.  $^{20-22}$ ).

To demonstrate the predictive power of our materials design principle, we have synthesized single-crystalline  $Ce_2Au_3In_5$  and its La counterpart,  $La_2Au_3In_5$ . The electronic specific heat of  $Ce_2Au_3In_5$  is shown in Fig. 4d (Supplementary Fig. 6 shows how the phonon contribution is determined). The low-temperature upturn indicates the influence of a (presumably magnetic) phase transition below the lowest measured temperature (2 K). In the paramagnetic regime free of this influence, a  $\Gamma T^2$  form is observed. Fitting  $\Gamma$  in terms of equation (2) (Supplementary Fig. 15) yields a nodal velocity  $v^*$  = 2994 m s<sup>-1</sup>. This represents a close to three orders of magnitude

NATURE PHYSICS ARTICLES

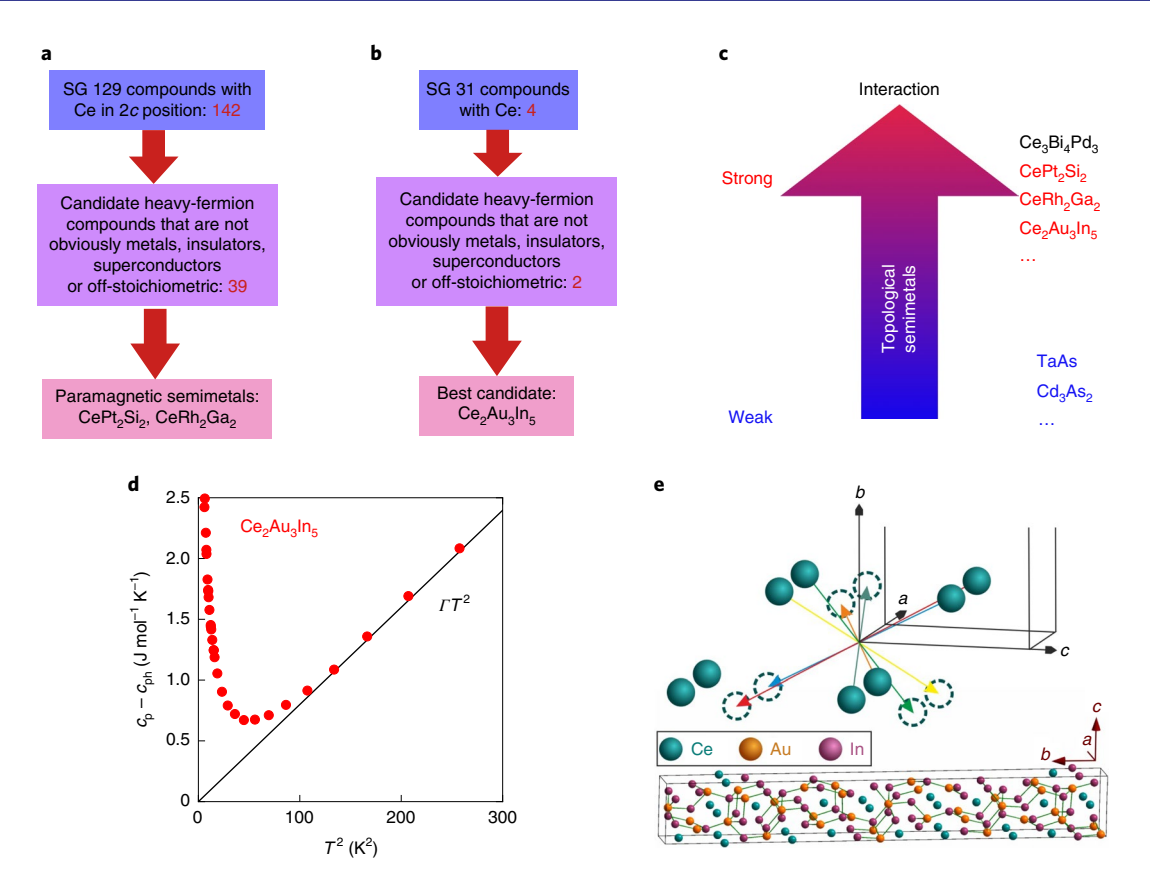


**Fig. 4 | Design of new materials for correlation-driven topological semimetal phases and the first synthesized material. a,b**, Design procedure as applied to SG 129 with Ce ions on the Wyckoff position 2c (**a**) and to SG 31 (**b**). The 39 compounds in **a** (middle) and the 4 compounds in **b** are shown in Supplementary Fig. 4. **c**, Summary of the newly identified candidate materials (red) for correlation-driven topological semimetals based on the search in **a** and **b** and their placement along the correlation axis. **d**, Electronic specific heat,  $c_p - c_{phr}$  as a function of  $T^2$ . In the paramagnetic regime sufficiently above the low-temperature upturn (possibly a tail of a lower-lying magnetic-phase transition), a  $\Gamma T^2$  form is observed. **e**, Crystal structure of Ce<sub>2</sub>Au<sub>3</sub>In<sub>5</sub> and illustration of its inversion-symmetry breaking.

renormalization from the typical velocity of non-interacting electrons, which is consistent with the association with Kondo-driven composite fermions.

Our approach for materials design can be readily generalized. For example, our procedure applies to other Wyckoff positions (for example, Ce ions at positions 2a or 2b instead of 2c), other lanthanide elements (Pr, Sm, Eu and Yb, in addition to Ce) and actinide elements (for example, U), and finally, a large number of other SG symmetries (in particular, those among the 155 non-symmorphic SGs). These factors make it probable that hundreds of candidate materials can be realized for strongly correlated topological semimetal phases.

We now underscore some general lessons drawn from our results. Our models have an even number of electrons per unit cell. The typical localizing tendency of strong correlations could have turned the systems into Kondo insulators 14,51,52. Instead, the strong correlations cooperate with the SG symmetries (Fig. 1a): the Kondo effect generates composite fermions; the SG symmetry constraints on the composite fermions prevent the Kondo gap from developing and instead lead to the Weyl nodal excitations.

Going beyond Kondo systems, emergent low-energy excitations can already develop for intermediate correlations when the correlation strength is comparable to the non-interacting bandwidth. Here, too, they will be subjected to SG symmetry constraints. To illustrate the point, consider a multi-orbital Hubbard model containing both Hubbard and Hund interactions and with the orbitals having unequal kinetic energies<sup>53,54</sup>. When a correlated metal develops near an orbital-selective Mott phase, the emergent low-energy excitations

take the form of a narrow band that is bound to the immediate vicinity of the Fermi energy, as indeed seen experimentally<sup>55</sup>. For such models, in suitable crystalline settings, the SG symmetries are expected to constrain the low-energy excitations and produce gapless topological phases. Thus, our work motivates parallel (and systematic) studies for correlated gapless electronic topology in such multi-orbital models and the associated transition metal compounds. We can expect our approach to provide a means for identifying hitherto-unknown phases and materials of correlated electronic topology in a variety of settings across a wide correlation spectrum. Finally, correlation physics that involves non-trivial electronic topology is a general problem that pertains to a growing list of materials. As recent studies<sup>56</sup> in the moiré bands of twisted bilayer graphene illustrate, the kind of topological heavy fermions we advance here may effectively serve as a platform to elucidate the enigmatic physics of these emerging materials.

Our work has advanced a materials design principle, namely, strong correlations cooperate with SG symmetry to drive correlated topological solids, as well as a general procedure to identify new materials for correlation-driven topological semimetals. Our findings illustrate the potential of the design principle to guide the search for new correlated topological metals in a broad range of strongly correlated quantum materials. Given that new materials and novel quantum phases may serve as anchoring points for new physics and unusual properties that are yet to be foreseen, we expect our work to guide the exploration of the vast landscape of metallic topological matter in strongly correlated regimes.

## f-core DFT calculations

The electronic structure calculations were performed with the f states removed from the pseudo-potential to model the band structure. The SOC was taken into account. Further details can be found in the 'Further details and additional results of the DFT calculations' in the Supplementary Information.

#### Online content

Any methods, additional references, Nature Research reporting summaries, source data, extended data, supplementary information, acknowledgements, peer review information; details of author contributions and competing interests; and statements of data and code availability are available at https://doi.org/10.1038/s41567-022-01743-4.

Received: 17 December 2021; Accepted: 18 July 2022; Published online: 15 September 2022

## References

- Keimer, B. & Moore, J. E. The physics of quantum materials. Nat. Phys. 13, 1045–1055 (2017).
- Paschen, S. & Si, Q. Quantum phases driven by strong correlations. Nat. Rev. Phys. 3, 9–26 (2021).
- 3. Cano, J. & Bradlyn, B. Band representations and topological quantum chemistry. *Annu. Rev. Condens. Matter Phys.* 12, 225–246 (2021).
- 4. Bradlyn, B. et al. Topological quantum chemistry. Nature 547, 298-305 (2017).
- Cano, J. et al. Building blocks of topological quantum chemistry: elementary band representations. *Phys. Rev. B* 97, 035139 (2018).
- Po, H. C., Vishwanath, A. & Watanabe, H. Symmetry-based indicators of band topology in the 230 space groups. *Nat. Commun.* 8, 50 (2017).
- Watanabe, H., Po, H. C., Zaletel, M. P. & Vishwanath, A. Filling-enforced gaplessness in band structures of the 230 space groups. *Phys. Rev. Lett.* 117, 096404 (2016).
- Castro Neto, A. H., Guinea, F., Peres, N. M. R., Novoselov, K. S. & Geim, A. K. The electronic properties of graphene. Rev. Mod. Phys. 81, 109–162 (2009).
- Fu, L., Kane, C. L. & Mele, E. J. Topological insulators in three dimensions. Phys. Rev. Lett. 98, 106803 (2007).
- Vergniory, M. G. et al. A complete catalogue of high-quality topological materials. *Nature* 566, 480–485 (2019).
- Zhang, T. et al. Catalogue of topological electronic materials. *Nature* 566, 475–479 (2019).
- Maciejko, J. & Fiete, G. A. Fractionalized topological insulators. Nat. Phys. 11, 385–388 (2015).
- Rachel, S. & Le Hur, K. Topological insulators and Mott physics from the Hubbard interaction. *Phys. Rev. B* 82, 075106 (2010).
- Dzero, M., Sun, K., Galitski, V. & Coleman, P. Topological Kondo insulators. Phys. Rev. Lett. 104, 106408 (2010).
- Schaffer, R., Lee, E. K.-H., Yang, B.-J. & Kim, Y. B. Recent progress on correlated electron systems with strong spin-orbit coupling. *Rep. Prog. Phys.* 79, 094504 (2016).
- Armitage, N. P., Mele, E. J. & Vishwanath, A. Weyl and Dirac semimetals in three-dimensional solids. Rev. Mod. Phys. 90, 015001 (2018).
- 17. Lai, H.-H., Grefe, S. E., Paschen, S. & Si, Q. Weyl-Kondo semimetal in heavy-fermion systems. *Proc. Natl Acad. Sci. USA* 115, 93–97 (2018).
- Grefe, S. E., Lai, H.-H., Paschen, S. & Si, Q. Weyl-Kondo semimetals in nonsymmorphic systems. *Phys. Rev. B* 101, 075138 (2020).
- Grefe, S. E., Lai, H.-H., Paschen, S. & Si, Q. Extreme topological tunability of Weyl-Kondo semimetal to Zeeman coupling. Preprint at https://arxiv.org/abs/ 2012.15841 (2020).
- Dzsaber, S. et al. Kondo insulator to semimetal transformation tuned by spin-orbit coupling. *Phys. Rev. Lett.* 118, 246601 (2017).
- Dzsaber, S. et al. Giant spontaneous Hall effect in a nonmagnetic Weyl-Kondo semimetal. Proc. Natl Acad. Sci. USA 118, e2013386118 (2021).
- Dzsaber, S. et al. Controlling electronic topology in a strongly correlated electron system. Preprint at https://arxiv.org/abs/1906.01182 (2019).
- Asaba, T. et al. Colossal anomalous Nernst effect in a correlated noncentrosymmetric kagome ferromagnet. Sci. Adv. 7, eabf1467 (2021).
- 24. Kang, M. et al. Dirac fermions and flat bands in the ideal kagome metal FeSn. *Nat. Mater.* **19**, 163–169 (2020).
- 25. Yao, M. et al. Switchable Weyl nodes in topological kagome ferromagnet Fe<sub>3</sub>Sn<sub>2</sub>. Preprint at https://arxiv.org/abs/1810.01514 (2018).
- 26. Morimoto, T. & Nagaosa, N. Weyl Mott insulator. Sci. Rep. 6, 19853 (2016).
- Wagner, N., Ciuchi, S., Toschi, A., Trauzettel, B. & Sangiovanni, G. Resistivity exponents in 3D Dirac semimetals from electron-electron interaction. *Phys. Rev. Lett.* 126, 206601 (2021).

- Lourenço, J. A. S., Eneias, R. L. & Pereira, R. G. Kondo effect in a PT
  -symmetric non-Hermitian Hamiltonian. Phys. Rev. B 98, 085126 (2018).
- Ahamed, S., Moessner, R. & Erten, O. Why rare-earth ferromagnets are so rare: insights from the p-wave Kondo model. Phys. Rev. B 98, 054420 (2018).
- 30. Jang, S. et al. Direct visualization of coexisting channels of interaction in CeSb. Sci. Adv. 5, eaat7158 (2019).
- Chiu, C.-K. & Schnyder, A. P. Classification of reflection-symmetry-protected topological semimetals and nodal superconductors. *Phys. Rev. B* 90, 205136 (2014).
- Bian, G. et al. Topological nodal-line fermions in spin-orbit metal PbTaSe<sub>2</sub>. Nat. Commun. 7, 10556 (2016).
- 33. Bian, G. et al. Drumhead surface states and topological nodal-line fermions in TITaSe, *Phys. Rev. B* **93**, 121113 (2016).
- Chan, Y.-H., Chiu, C.-K., Chou, M. Y. & Schnyder, A. P. Ca<sub>3</sub>P<sub>2</sub> and other topological semimetals with line nodes and drumhead surface states. *Phys. Rev. B* 93, 205132 (2016).
- Young, S. M. & Kane, C. L. Dirac semimetals in two dimensions. *Phys. Rev. Lett.* 115, 126803 (2015).
- Schoop, L. M. et al. Dirac cone protected by non-symmorphic symmetry and three-dimensional Dirac line node in ZrSiS. Nat. Commun. 7, 11696 (2016).
- 37. Schoop, L. M. et al. Tunable Weyl and Dirac states in the nonsymmorphic compound CeSbTe. Sci. Adv. 4, eaar2317 (2018).
- 38. Muechler, L. et al. Modular arithmetic with nodal lines: drumhead surface states in ZrSiTe. *Phys. Rev. X* **10**, 011026 (2020).
- Klemenz, S., Schoop, L. & Cano, J. Systematic study of stacked square nets: from Dirac fermions to material realizations. *Phys. Rev. B* 101, 165121 (2020).
- Nica, E. M., Yu, R. & Si, Q. Glide reflection symmetry, Brillouin zone folding, and superconducting pairing for the P4/nmm space group. Phys. Rev. B 92, 174520 (2015).
- Li, C. et al. Rules for phase shifts of quantum oscillations in topological nodal-line semimetals. Phys. Rev. Lett. 120, 146602 (2018).
- 42. Yang, H., Moessner, R. & Lim, L.-K. Quantum oscillations in nodal line systems. *Phys. Rev. B* **97**, 165118 (2018).
- 43. Kwan, Y. H. et al. Quantum oscillations probe the Fermi surface topology of the nodal-line semimetal CaAgAs. *Phys. Rev. Res.* 2, 012055 (2020).
- Stuart, B. A. et al. Quasiparticle interference observation of the topologically nontrivial drumhead surface state in ZrSiTe. *Phys. Rev. B* 105, L121111 (2022)
- Biderang, M., Leonhardt, A., Raghuvanshi, N., Schnyder, A. P. & Akbari, A. Drumhead surface states and their signatures in quasiparticle scattering interference. *Phys. Rev. B* 98, 075115 (2018).
- Kirchner, S. et al. Colloquium: heavy-electron quantum criticality and single-particle spectroscopy. Rev. Mod. Phys. 92, 011002 (2020).
- Anand, V. K., Adroja, D. T., Bhattacharyya, A., Klemke, B. & Lake, B. Kondo lattice heavy fermion behavior in CeRh<sub>2</sub>Ga<sub>2</sub>. *J. Phys. Condens. Matter* 29, 135601 (2017).
- Gignoux, D., Schmitt, D., Zerguine, M., Ayache, C. & Bonjour, E. Magnetic properties of a new Kondo lattice compound: CePt<sub>2</sub>Si<sub>2</sub>. *Phys. Lett. A* 117, 145–149 (1986).
- Nakamoto, G. et al. Crystal growth and characterization of the Kondo semimetal CeNiSn. J. Phys. Soc. Jpn 64, 4834–4840 (1995).
- Galadzhun, Y. V., Hoffmann, R.-D., Pöttgen, R. & Adam, M. Complex three-dimensional [Au<sub>3</sub>In<sub>5</sub>] polyanions in Ln<sub>2</sub>Au<sub>3</sub>In<sub>5</sub> (Ln = Ce, Pr, Nd, Sm). J. Solid State Chem. 148, 425–432 (1999).
- Aeppli, G. & Fisk, Z. Kondo insulators. Comments Condens. Matter Phys. 16, 155–165 (1992).
- Nikolić, P. Two-dimensional heavy fermions on the strongly correlated boundaries of Kondo topological insulators. *Phys. Rev. B* 90, 235107 (2014).
- Yu, R. & Si, Q. Orbital-selective Mott phase in multiorbital models for iron pnictides and chalcogenides. *Phys. Rev. B* 96, 125110 (2017).
- Komijani, Y. & Kotliar, G. Analytical slave-spin mean-field approach to orbital selective Mott insulators. *Phys. Rev. B* 96, 125111 (2017).
- Huang, J. et al. Correlation-driven electronic reconstruction in FeTe<sub>1-x</sub>Se<sub>x</sub>. Commun. Phys. 5, 29 (2022).
- Song, Z.-D. & Bernevig, B. A. MATBG as topological heavy fermion: I. Exact mapping and correlated insulators. Preprint at https://arxiv.org/abs/2111.05865 (2021).

**Publisher's note** Springer Nature remains neutral with regard to jurisdictional claims in published maps and institutional affiliations.

Springer Nature or its licensor holds exclusive rights to this article under a publishing agreement with the author(s) or other rightsholder(s); author self-archiving of the accepted manuscript version of this article is solely governed by the terms of such publishing agreement and applicable law.

© The Author(s), under exclusive licence to Springer Nature Limited 2022

NATURE PHYSICS ARTICLES

### Methods

Periodic Anderson model, solution method and symmetry analyses. The periodic Anderson model is specified by equation (1). The model contains two species of spin-1/2 electrons. The Hamiltonian  $\mathcal{H}_d$ , containing spin-1/2 d operators, describes the physical localized f electrons:

$$\mathcal{H}_{d} = E_{d} \sum_{i,\sigma} d^{\dagger}_{i\sigma} d_{i\sigma} + U \sum_{i} n^{d}_{i\uparrow} n^{d}_{i\downarrow}, \tag{3}$$

where  $E_d$  is the energy level and U is the onsite Coulomb repulsion. However,  $\mathcal{H}_c$ , which involves c operators, characterizes the spd conduction electrons that form the non-interacting bands. The hybridization term, which describes the Kondo coupling between the conduction and f electrons, is given by

$$\mathcal{H}_{cd} = V \sum_{i\sigma} \left( d_{i\sigma}^{\dagger} c_{i\sigma} + \text{h.c.} \right),$$
 (4)

where V represents the hybridization between the two species of electrons. The following features of SG 129 and model justify its application to many f-electron materials in this SG. The symmetry representations of this SG are such that at each high-symmetry point, the degeneracy of the bands is independent of the symmetry of the orbital (assuming SOC). Thus, our model applies regardless of the nature of the orbitals near the Fermi energy. The dispersion of Kondo-driven composite fermions stays near the Fermi energy, within the Kondo energy. Thus, although we specialize in the quarter-filled case (corresponding to one electron per site), changing the filling will only shift the composite-fermion bands up to the Kondo energy. The saddle-point analysis, involving self-consistent equations that are exact in a large-N limit (where N is the spin degeneracy), is described in the Supplementary Information. The Kondo effect generates composite fermions that must be located near the Fermi energy. Although we will describe symmetry constraints in terms of the dispersion of composite fermions, the same conclusion is reached through a more general analysis that is carried out in terms of the eigenvectors of the full singleparticle Green's function for the interacting Hamiltonian<sup>57</sup> (see the 'Symmetry analysis of the interacting Green's function' section in the Supplementary Information).

The periodic Anderson model in 2D involves

$$\mathcal{H}_{c} = \sum_{\mathbf{k}} \Psi_{\mathbf{k}}^{\dagger} H_{c}(\mathbf{k}) \Psi_{\mathbf{k}},$$

where  $\Psi_{\mathbf{k}}^{\mathrm{T}}=(c_{\mathbf{k}\uparrow A},c_{\mathbf{k}\downarrow A},c_{\mathbf{k}\uparrow B},c_{\mathbf{k}\downarrow B})$ . Furthermore,

$$H_{c}(\mathbf{k}) = t_{1} \cos \frac{k_{x}}{2} \cos \frac{k_{y}}{2} \tau_{x} + t_{2} (\cos k_{x} + \cos k_{y}) + t^{SO} (\sin k_{x} \sigma_{y} - \sin k_{y} \sigma_{x}) \tau_{z}$$

$$+ \Delta \sin \left(\frac{k_{x} - k_{y}}{2}\right) \tau_{x} \sigma_{z},$$

$$(5)$$

where  $\mathbf{\tau} = (\tau_x, \tau_y, \tau_z)$  and  $\mathbf{\sigma} = (\sigma_x, \sigma_y, \sigma_z)$  are Pauli matrices acting on the (A, B)sublattice and spin spaces, respectively. A more explicit form of the Hamiltonian can be found in the Supplementary Information ('Hamiltonians in matrix form' section). For definiteness, we consider the lattice model with tight-binding hopping terms between the nearest  $(t_1)$  and next-nearest  $(t_2)$  sites (Supplementary Fig. 3a), an SOC ( $t^{SO}$ ) term and an inversion-symmetry-breaking ( $\Delta$ ) term. The first three terms contain all the symmetry-allowed components up to the next-nearest neighbour, describing an effective s-orbital model on Wyckoff position 2c with both time-reversal symmetry ( $\mathcal{T}$ ) and inversion symmetry ( $\mathcal{I}$ ). The presence of both  $\mathcal{T}$  and  $\mathcal{I}$  ensure each band is doubly degenerate with states  $|g\rangle$  and  $\mathcal{TI}|g\rangle$ . In addition, the symmetries include the glide mirror symmetry  $\{M_z | \frac{1}{2}, \frac{1}{2}\}$  (Fig. 1b,c) and two screw symmetries  $\{C_{2x}|\frac{1}{2}0\}$  and  $\{C_{2y}|0\frac{1}{2}\}$  (where  $\{C_{ni}|\mathbf{t}\}$  is the *n*-fold rotation along axis i + fractional translation t; Fig. 1c). The bands are generically twofold degenerate. However, a fourfold degeneracy at X arises as a result of either the mirror non-symmorphic  $\{M_z | \frac{1}{2}, \frac{1}{2}\}$  symmetry or the screw non-symmorphic  $\{C_{2x}|\frac{1}{2}0\}$  symmetry. The same degeneracy appears at Y, due to either the mirror non-symmorphic  $\{M_z|\frac{1}{2},\frac{1}{2}\}$  symmetry or the screw non-symmorphic  $\{C_{2y}|0\frac{1}{2}\}$  symmetry. Finally, a fourfold degeneracy also develops at M, from either the  $\{C_{2x}|\frac{1}{2}0\}$  or the  $\{C_{2y}|0\frac{1}{2}\}$  symmetry. The fourth term has the form of  $\Delta \sin(\frac{k_x - k_y}{2}) \tau_x \sigma_z$ . It breaks the inversion symmetry of p4/nmm and preserves its mirror symmetry<sup>35,58</sup>. The quarter-filling case we examine corresponds to one electron per site. We consider the realistic regime of parameters corresponding to the limit of strong coupling,  $U \rightarrow \infty$ , and with the *d*-electron level being sufficiently deep compared with the energy of the conduction-electron bands (that is, for sufficiently negative  $E_d$ ), in which the system is in the Kondo limit. The saddle-point analysis results are compatible with those derived from a variety of other methods. For example, the Kondo effect is found to develop only when the hybridization strength goes above a threshold value. This reflects the fact that the bare conduction-electron bath has a gap near the Fermi energy. The gap makes the Kondo coupling to be irrelevant (as opposed to marginally relevant) in the renormalization-group sense; as a result, a non-zero threshold value of the Kondo coupling or hybridization is needed for the Kondo effect to develop.

We now specify the periodic Anderson model in three dimensions. Here  $\mathcal{H}_d$  and  $\mathcal{H}_{cd}$  are the same (except that the site summation is in the 3D lattice). For the conduction electrons, the Hamiltonian now takes the form  $\mathcal{H}_c^{\mathrm{3D}} = \sum_{\mathbf{k}} \boldsymbol{\phi}_{\mathbf{k}}^{\mathrm{T}} \boldsymbol{H}_c^{\mathrm{3D}}(\mathbf{k}) \boldsymbol{\Phi}_{\mathbf{k}}$ , where  $\boldsymbol{\Phi}_{\mathbf{k}}^{\mathrm{T}} = (c_{\mathbf{k}\uparrow A}^{\mathrm{s}}, c_{\mathbf{k}\downarrow A}^{\mathrm{s}}, c_{\mathbf{k}\downarrow B}^{\mathrm{s}}, c_{\mathbf{k}\downarrow A}^{\mathrm{p}}, c_{\mathbf{k}\downarrow A}^{\mathrm{p}}, c_{\mathbf{k}\downarrow B}^{\mathrm{p}}, c_{\mathbf{k}\downarrow B}^{\mathrm{p}})$ . In this equation,  $H^{\mathrm{3D}}(\mathbf{k})$ 

$$=H_c(k_x,k_y)\otimes\rho_z+\Delta_z\rho_z+t_z^1\sin(\frac{k_z}{2})\rho_y+t_z^2\cos(k_z)\rho_z+m_z\tau_x\otimes\sigma_x\otimes\rho_y,$$
(6)

where  $\rho_{x,y,z}$  denote the Pauli matrices in the space of the two stacking layers (the 'Hamiltonians in matrix form' section in the Supplementary Information provides a more explicit form of the Hamiltonian). Here the third and fourth terms represent the nearest- and next-nearest-neighbour hoppings along the z direction (Supplementary Fig. 3a) and the fifth term is the SOC along the z direction. For simplicity, we have chosen s- and p-orbital stacking and set the s- and p- orbitals to couple with the d- electrons with the same hybridization strength. However, the nature of the resulting topological semimetal phase is determined by the underlying SG symmetry and is generic to the given SG. Further details of our analysis is described in the Supplementary Information and Supplementary Fig. 3. Again, we focus on the quarter-filling case.

Crystal growth and specific heat of Ce2Au3In5 and La2Au3In5. Single crystals of Ce<sub>2</sub>Au<sub>3</sub>In<sub>5</sub> were grown from In flux using alumina crucibles. Elements of high purity (>99.9%) were taken for the synthesis. Single crystals were separated from the melt by centrifuging. Attempts to prepare single crystals of La2Au3In5 by this way failed. A single-phase polycrystalline La₂Au₃In₅ sample was prepared by melting pure elements in the stoichiometric ratio in a high-frequency furnace and annealing the as-cast sample at 650 °C for three days. All the samples were analysed by X-ray powder diffraction and energy-dispersive X-ray spectroscopy for phase purity and composition before the physical property measurements. The single crystallinity of the Ce<sub>2</sub>Au<sub>3</sub>In<sub>5</sub> samples was checked by Laue X-ray measurements. The specific heat  $c_p$  was measured using the Quantum Design heat capacity option for the physical property measurement system. Supplementary Fig. 6a shows the  $c_p$  value of Ce<sub>2</sub>Au<sub>3</sub>In<sub>5</sub> and La<sub>2</sub>Au<sub>3</sub>In<sub>5</sub> as a function of  $T^3$ . The phonon contribution to specific heat  $(c_{ph})$ , assumed as usual to be the same for both compounds, was estimated from the c, value of La2Au3In5 by subtracting its electronic contribution, determined as follows: the  $c_p/T$  value of La<sub>2</sub>Au<sub>3</sub>In<sub>5</sub> at low temperatures (<5 K) is well described by a conventional Debye–Sommerfeld model, namely,  $c_p/T = \gamma + \beta T^2$ (Supplementary Fig. 6b). It yielded a finite electronic specific-heat coefficient  $\gamma = (16.2 \pm 0.6) \,\mathrm{mJ} \,\mathrm{mol}^{-1} \,\mathrm{K}^{-2}$  and a  $\beta$  value that corresponds to the Debye temperature (232 ± 5) K. The electronic specific heat of Ce<sub>2</sub>Au<sub>3</sub>In<sub>5</sub> was obtained by subtracting  $c_{ph}$  from its total  $c_p$ .

## Data availability

The data that support the findings of this study are available from the corresponding authors upon reasonable request. Source data are provided with this paper.

## Code availability

The computer codes that were used to generate the data that support the findings of this study are available from the corresponding authors upon reasonable request.

## References

- 57. Hu, H. et al. Gapless electronic topology without free-electron counterpart. Preprint at https://arxiv.org/abs/2110.06182 (2021).
- Wu, W. et al. Hourglass Weyl loops in two dimensions: theory and material realization in monolayer GaTeI family. Phys. Rev. Mater. 3, 054203 (2019).

#### Acknowledgements

The work at Rice has been supported by the Air Force Office of Scientific Research under grant no. FA9550-21-1-0356 (C.S. and Q.S.), the National Science Foundation (NSF) under grant no. DMR-2220603 (L.C.) and the Robert A. Welch Foundation grant no. C-1411 (H.H.). The majority of the computational calculations have been performed on the Shared University Grid at Rice funded by NSF under grant EIA-0216467, a partnership between Rice University, Sun Microsystems and Sigma Solutions; the Big-Data Private-Cloud Research Cyberinfrastructure MRI award funded by NSF under grant no. CNS-1338099; and the Extreme Science and Engineering Discovery Environment (XSEDE) by NSF under grant no. DMR170109. M.G.V. acknowledges support from the Spanish Ministry of Science and Innovation grant no. PID2019-109905GB-C21 and the Deutsche Forschungsgemeinschaft (DFG, German Research Foundation) GA 3314/1-1-FOR 5249 (QUAST). The work at Los Alamos was carried out under the auspices of the US Department of Energy (DOE) National Nuclear Security Administration under contract no. 89233218CNA000001, and was supported by LANL LDRD program. J.C. acknowledges support from the NSF under grant no. DMR-1942447

and support from the Flatiron Institute, a division of the Simons Foundation. The work in Vienna was supported by the Austrian Science Fund (project nos. 29279-N27 and I 5868-N-FOR 5249—QUAST). S.G., S.P., J.C. and Q.S. acknowledge the hospitality of the Aspen Center for Physics, which is supported by NSF grant no. PHY-1607611.

## **Author contributions**

Q.S., J.C. and S.P. conceived the research. L.C., C.S., H.H., S.E.G., J.C. and Q.S. carried out the theoretical model studies. A.P. and S.P. identified the candidate materials for the proposed correlated topological semimetals. L.F. and X.Y. synthesized the material and G.E. performed the specific-heat measurements. M.G.V. performed the DFT calculations. L.C., C.S., H.H., J.C. and Q.S. wrote the manuscript, with inputs from all the authors.

## **Competing interests**

The authors declare no competing interests.

## **Additional information**

**Supplementary information** The online version contains supplementary material available at https://doi.org/10.1038/s41567-022-01743-4.

**Correspondence and requests for materials** should be addressed to Silke Paschen, Jennifer Cano or Qimiao Si.

**Peer review information** *Nature Physics* thanks Johann Kroha and the other, anonymous, reviewer(s) for their contribution to the peer review of this work.

Reprints and permissions information is available at www.nature.com/reprints.